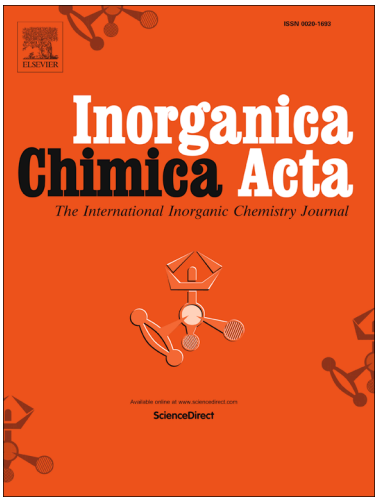

Research paper

Functional models for type-2 and type-3 copper oxidases: Self-assembled molecular association in [Cu(L)(Hdpa)](ClO_4) determines the catalytic activity

Velusamy Sathya, Mariappan Murali

PII: S0020-1693(18)31343-4
DOI: https://doi.org/10.1016/j.ica.2019.119016
Article Number: 119016
Reference: ICA 119016

To appear in: *Inorganica Chimica Acta*

Received Date: 16 August 2018
Revised Date: 10 June 2019
Accepted Date: 10 July 2019

Please cite this article as: V. Sathya, M. Murali, Functional models for type-2 and type-3 copper oxidases: Self-assembled molecular association in [Cu(L)(Hdpa)](ClO_4) determines the catalytic activity, *Inorganica Chimica Acta* (2019), doi: https://doi.org/10.1016/j.ica.2019.119016

Functional models for type-2 and type-3 copper oxidases: Self-assembled molecular association in [Cu(L)(Hdpa)](ClO_4) determines the catalytic activity

Velusamy Sathya and Mariappan Murali*

Coordination and Bioinorganic Chemistry Research Laboratory
Department of Chemistry
National College (Autonomous)
Tiruchirappalli 620 001
Tamil Nadu, India

e-mail: ma66mu@gmail.com

Phone: +91-431-2482995 / Fax: +91-431-2481997

Abstract

Mononuclear copper(II) complex [Cu(L)(Hdpa)](ClO_4) (**1**), where H(L) is tridentate NNO donor ligand and Hdpa is 2,2'-dipyridylamine has been isolated. The X-ray crystal structure of **1** possesses a CuN_4O chromophore with square pyramidal (4+1) coordination geometry. It displays self-assembled molecular association viz., (a) intermolecular N-H···O hydrogen bonding and (b) inter-pair π-π anti-parallel stacking. The complex is catalytically effective in the oxidation of benzylamine to benzaldehyde and 3,5-di-*tert*-butylcatechol to 3,5-di-*tert*-butyl-*o*-quinone, thus act as a functional model for amine oxidase and catechol oxidase respectively.

1. Introduction

Copper containing metalloproteins in the living system plays a fundamental role in revealing its catalytic role as dioxygen and/or substrates activators towards different bio-function [1]. In this context, chemists have significantly contributed in unveiling the mystery of nature, especially by designing different metal complexes which can potentially mimic the active site and/or function of different copper proteins in nature [2,3]. One of the important copper oxidases is ascorbate oxidase (AO), consisting of three types of copper centers in which the type-2 copper site ($A_{\|} > 140 \times 10^{-4}$ cm^{-1}) belongs to the functional trinuclear cluster [4], coordinated to two histidine molecules and a water molecule. The primary role of the type-2 copper center is electron transfer, in which ascorbate under physiological reaction conditions acts as an electron donor. The reduced copper(I) sites activate dioxygen and convert it to water involving four electrons and four protons in AO [5]. The amine oxidase (AmO) is another type-2 copper oxidase, which arises as homodimers. The active site of each subunit contains one copper center [6] coordinated with three histidine residues and two water molecules in a distorted square pyramidal geometry. It is responsible for two-electron oxidation of primary amines to aldehydes [7]. Catechol oxidase (CO), catalyzes the oxidation of catechol to *o*-quinone accompanying the four electron reduction of O_2 to H_2O [8]. The CO is a type-3 copper protein containing dicopper center coordinated by six histidine nitrogen atoms and μ-η^2:η^2 peroxo-bridged *oxy* form [9-11].

Many model complexes with dicopper center (Cu···Cu ≤ 5 Å) mimic the copper oxidases [12-14], both structurally and functionally whereas the same for the monocopper center counterparts remain uncommon. Several works in the literature indicates that the efficiency of a mononuclear copper(II) complex as catalyst in copper oxidase activity [15-20] have been influenced by a number of factors such as nature of square pyramidal (4+1) coordination geometry, labile binding sites, chelate ring size, nature of the donor groups, electronic properties of the ligands, existence of self-assembled molecular association to form mononuclear pairs, Cu···Cu separation, redox potentials from electrochemical studies and steric match between the substrate and catalyst. All these facts reflect that explorations of the possibility of exhibiting copper oxidase activity by new types of compounds are very much demanding, and our research group is engaged in this endeavor. In the present work, green colored mononuclear copper(II) complex (Scheme 1) has been synthesized, characterized and its potential catalytic activity has been tested with an aim to mimic functional sites of ascorbate, amine and catechol oxidases.

2. Experimental Section

2.1. Materials

Copper(II) acetate monohydrate, 2,2'-dipyridylamine, 2-hydroxy-1-naphthaldehyde, sodium perchlorate, *N*,*N*-dimethylethylenediamine, 3,5-di-*tert*-butylcatechol, *tetra*-*N*-butylammonium bromide (Sigma-Aldrich), L-ascorbic acid (Fisher Scientific), benzylamine (Avra), KI, ammonium molybdate and hydrogen peroxide solution (30% w/v) (Merck) were used as received. HPLC grade methanol, *N*,*N*-dimethylformamide, ethyl acetate, hexane, dichloromethane and acetonitrile and reagent grade diethyl ether were purchased from Merck.

2.2. Physical Measurements

Microanalyses (C, H, and N) were carried out with a Vario EL elemental analyzer. The conductivity is measured using EQUIPTRONICS EQDCMP bridge with a solute concentration of 1×10^{-3} M in MeOH. Mass spectrometry was performed on a ZQ ESI-MS spectrometer. Magnetic susceptibility data at 27 °C were obtained for polycrystalline samples using George Associates Inc. FTIR spectra were recorded using a Perkin Elmer Spectrum RX1 FTIR spectrophotometer in the range 400-4000 cm^{-1} with a sample prepared as KBr disc. UV-Visible spectroscopy of reflectance spectra was recorded using Shimadzu UV-2450 UV-VIS spectrophotometer and solution spectra were recorded using Perkin Elmer Lambda-365 UV-VIS spectrophotometer using cuvettes of 1 cm path length. X-band EPR spectra of the complex in DMF, MeOH and MeCN at liquid nitrogen temperature (77 K) and polycrystalline at room

temperature (RT) were recorded on a JEOL JES-FA200 ESR spectrometer. ^{1}H NMR spectra were recorded on a Bruker 300 MHz with AVANCE II NMR spectrometer in $CDCl_3$. Cyclic voltammetry (CV) and differential pulse voltammetry (DPV) on glassy carbon electrode were performed in MeOH 25 ± 0.2 °C. The voltammograms were generated using CH instruments 620C electrochemical analyzer. A three electrode system has been used to study the electrochemical behavior of complexes (0.001 M) consisting of a glassy carbon working electrode (A = 0.0707 cm^2), a platinum wire auxiliary electrode and saturated calomel reference electrode and TBAP (0.1 M) is used as a supporting electrolyte. Solutions were deoxygenated by purging with nitrogen gas for 15 min prior to the measurements.

*2.3. Synthesis of [Cu(L)(Hdpa)](ClO$_4$) (**1**)*

The complex **1** was prepared [21] by the reaction of $Cu(O_2CMe)_2.H_2O$ (0.20 g, 1 mmol) with 2,2'-dipyridylamine (Hdpa; 0.17 g, 1 mmol) in methanol (15 mL). The mixture was left stirring for 1 h at 25 °C at which point the yellow solution of H(L), obtained from the condensation of 2-hydroxy-1-naphthaldehyde (0.17 g, 1 mmol) and *N*,*N*-dimethylethylenediamine (0.09 g, 1 mmol) [22,23], was added. The resultant green solution was refluxed for 3 h. The green solids obtained after the addition of a methanolic solution of $NaClO_4$ (0.122 g, 1 mmol) were filtered and dried in *vacuo* over P_4O_{10}. Yield: 0.35 g (61 %). Anal. Calcd. for $C_{25}H_{26}N_5O_5ClCu$ (**1**): C, 52.18; H, 4.55; N, 12.17 %. Found: C, 52.24; H, 4.46; N, 12.13 %. Λ_M: 75 (MeOH) Ω^{-1} cm^2 mol^{-1}. ESI-MS (MeCN): m/z 475.17 [M^+-ClO_4]. μ_{eff} (27 °C): 1.8 μB. FT-IR (KBr, cm^{-1}) selected bands: 1622 ν_{imine}(C=N), 1584 ν_{py}(C=N), 1305 ν(naph-O), 1092, 621 $\nu(ClO_4^-)$. Electronic spectrum in solid/MeOH [λ_{max}/nm (ε_{max}/dm^3 mol^{-1} cm^{-1})]: 653/651 (202), 897 sh (70), 393 (6802), 310 (28702), 260 (41118), 249 (44597). Electronic spectrum in MeOH:H_2O (4:1 v/v) [λ_{max}/nm (ε_{max}/dm^3 mol^{-1} cm^{-1})]: 649 (179), 891 sh (64), 389 (6414), 310 (26739), 261 (37863), 249 (40542). Polycrystalline EPR spectrum at RT: g_{iso} = 2.078. EPR spectrum in DMF solution at 77 K: $g_{\|}$ = 2.227, $g_{\perp}$ = 2.045, $A_{\|}$ = 188 × 10^{-4} cm^{-1}, $g_{\|}/A_{\|}$ = 118 cm, G = 5.2, α^2 = 0.80, β^2 = 0.65, γ^2 = 0.50, $K_{\|}$ = 0.72, $K_{\perp}$ = 0.63. EPR spectrum in MeOH solution at 77 K: g_{iso} = 2.128. EPR spectrum in MeCN solution at 77 K: g_{iso} = 2.083. Redox behavior in MeOH (0.1 M TBAP): CV, $E_{1/2}$ = 0.159 V, ΔE_p = 67 mV, i_{pa}/i_{pc} = 2.4 (decreases towards unity with increase in scan rate), D = 5.2 × 10^{-6} cm^2 s^{-1}; DPV, $E_{1/2}$ = 0.152 V.

2.4. X-ray structure determination

The green single crystal of [Cu(L)(Hdpa)](ClO$_4$) (**1**) suitable for X-ray structural determination was obtained by cooling a solution of **1** in MeOH:MeCN at 5 °C for five days. A green single crystal of **1** with dimensions 0.30 × 0.25 × 0.20 mm^3, was selected under the

polarizing microscope and then mounted on the glass fiber. The crystal data collections were performed through a Bruker AXS-KAPPA APEX II diffractometer using graphite monochromated Mo-K_α radiation (λ = 0.71073 Å). Cell parameters were retrieved using Bruker SMART software and refined using Bruker SAINT on all observed reflections [24]. Absorption corrections were performed using SADABS [24]. Structure solution was performed using direct methods with the program SHELXT-2014/4 and refined by full-matrix least squares on F^2 using SHELXL-2014/7 [25,26]. The C(1), C(2), C(3) and C(4) atoms in *N*,*N*-dimethylethylenediamine moiety of H(L) ligand and O(2), O(3), O(4) and O(5) atoms in perchlorate anion are twofold disordered. The components of disorder were located in difference Fourier map and refined with restraints on bond distances. Also, the sum of occupancies of the components (C, 0.544(6) and 0.456(6) and O, 0.342(9) and 0.658(9)) was restrained as 1. The non-hydrogen atoms were refined with anisotropic displacement parameters. All hydrogen atoms except the one belonging to a nitrogen atom (N4) were geometrically fixed at chemically meaningful positions. The N4 hydrogen atom could be located in a difference map and was refined isotropically without restraints.

2.5. Oxidation of ascorbic acid

The ascorbate oxidase activity of the complex is evaluated by reaction with **1** (3×10^{-3} M) and different concentration of ascorbic acid (H_2A). The experiments were run under aerobic conditions in MeOH:H_2O (4:1 v/v) medium and monitored using UV-Vis spectroscopy.

2.6. Oxidation of benzylamine

The catalytic action of **1** (1×10^{-3} M) in the H_2O_2 (1 ml of 30% w/v) dependent deamination of benzylamine (100×10^{-3} M) in 10 ml MeOH:H_2O (4:1 v/v) results in the oxidation of benzylamine to benzaldehyde. The organic products were isolated from the reaction mixture by solvent extraction with diethyl ether after removal of methanol. Diethyl ether was removed by rotary evaporation and the residue was dissolved in $CDCl_3$ and MeOH for ^{1}H NMR and ESI-MS measurements.

2.7. Kinetics of 3,5-di-tert-butylcatechol oxidation

To determine the catecholase activity of the complex, 2.9×10^{-5} M solution of the copper complex (**1**) in methanol was treated with 50 equivalents of 3,5-di-*tert*-butylcatechol (3,5-DTBC) in methanol under aerobic condition. The UV spectra of the solution were recorded directly after the addition and subsequently after regular intervals of 30 min and absorption value at 393 nm were measured as a function of time over a period of 3 h. To determine the dependence of the rates on the substrate concentration and various kinetic parameters, 2.9×10^{-5}

M solution of **1** was treated with 5-45 equivalents of 3,5-DTBC in methanol under aerobic condition.

To detect the formation of hydrogen peroxide during the catalytic reaction, reaction mixtures were prepared as in the kinetic experiments. During the course of the oxidation reaction, the solution was acidified with H_2SO_4 to pH 2 to stop further oxidation after a certain time and an equal volume of water was added. The formed quinine was extracted three times with dichloromethane. To the aqueous layer were added 1 mL of a 10% solution of KI and three drops of a 3% solution of ammonium molybdate. The formation of I_3^- could be monitored spectrophotometrically because of the development of the characteristic I_3^- band (λ = 353 nm, ε = 26000 M^{-1} cm^{-1}).

3. Results and Discussion

3.1. Synthesis and general aspects

Complex **1** was synthesized from 2,2'-dipyridylamine (Hdpa), Schiff base ligand H(L) (derived from the condensation of 2-hydroxy-1-naphthaldehyde and *N*,*N*-dimethylethylenediamine) and $Cu(O_2CMe)_2.H_2O$ and isolated as green colored crystals in good yield (~60%). The ESI-MS data in MeCN (m/z [M^+-ClO_4], 475.17) reveal that the complex retains its identity even in solution and this is supported by the value of molar conductivity in methanol (75 $\Omega^{-1}cm^2mol^{-1}$) for 1:1 electrolyte [20]. The complex exhibits infrared spectral band due to ν_{imine}(C=N) (1622 cm^{-1}), ν_{py}(C=N) (1584 cm^{-1}) and ν(naph-O) (1305 cm^{-1}), implying direct coordination of imine and pyridine nitrogen and naphtholate oxygen donors to copper(II). A broad intense band (1092 cm^{-1}) and a strong sharp band (621 cm^{-1}) are observed, which are characteristic of non-coordinated perchlorate ion. Based on the elemental analysis the complex was formulated as [Cu(L)(Hdpa)](ClO_4), which was confirmed by single crystal X-ray determination of **1**.

3.2. Description of the structure

The crystal refinement data and bond lengths and bond angles are listed in Tables 1 and 2 respectively and an ORTEP drawing of the complex cation $[Cu(L)(Hdpa)]^+$ (**1**) is shown in Fig. 1a. The Cu(II) cation is coordinated by naphtholate oxygen atom O(1) and two nitrogen atoms N(1) and N(2) of the Schiff base ligand, H(L) and two nitrogen atoms N(3) and N(5) of the Hdpa co-ligand. The value of the trigonality index τ (0.12) reveals that the coordination geometry around copper(II) is best described as distorted square pyramidal [20, 27]. The imine N(1) and amine N(2) nitrogen atoms and the naphtholate oxygen atom O(1) of the meridionally

coordinated Schiff base ligand and one of the imine nitrogen atom N(3) of Hdpa occupy the corners of the CuN_3O square plane of this geometry. The copper is displaced by 0.278(9) Å from the N_3O plane towards the axially coordinated nitrogen atom N(5) of Hdpa. Thus, axial position is occupied by nitrogen atom N(5) at a distance 2.1805(18) Å, longer than equatorial atoms (Cu(1)-O(1), 1.9567(15) Å; Cu(1)-N(1), 1.9230(18) Å; Cu(1)-N(2), 2.1338(19) Å; Cu(1)-N(3), 1.9979(18) Å) as a consequence of the presence of two electrons in d_{z^2} orbital of copper(II). The improper orientation of the lone pair on N(2) nitrogen of $-NMe_2$ group towards the $d_{x^2-y^2}$ orbital also would contribute to the longer Cu(1)-N(2) bond distance. The Cu-N_{amine} bond (Cu(1)-N(2), 2.1338(19) Å) is longer than the Cu-N_{imine} bond (Cu(1)-N(1), 1.9230(18) Å) formed by the Schiff base ligand, which is expected of sp^3 and sp^2 hybridizations of the amine N(2) and imine N(1) nitrogen atoms respectively. The degree of distortion is more towards square pyramidal due to smaller trigonality index, which could be related to (i) the two six-membered chelate rings Cu(1)O(1)C(15)C(6)C(5)N(1) and Cu(1)N(3)C(20)N(4)C(21)N(5) and the chelate ring, Cu(1)O(1)C(15)C(6)C(5)N(1) consists of Cu center bonded by the oxygen atom O(1) and nitrogen atom N(1) of the H(L) Schiff base ligand is nearly coplanar (0.011(3) Å) and (ii) the smaller dihedral angle (5.41(3)°) between the two coordinated pyridine rings of Hdpa.

Crystal packing reveals that cations of adjacent molecules are arranged in dimeric association (Fig. 1b). These pairs are held together by (a) intermolecular N-H···O hydrogen bonding and (b) inter-pair π-π interaction. The significant structural observation is the strongest intermolecular interaction leading to a centrosymmetric dimer (symmetry code: 2-x, -y, 1-z) in the crystal, is a N(4)-H(4)···O(1) hydrogen bond existing between the amine proton, H(4)(N4) of Hdpa and coordinated naphtholate oxygen O(1) (N(4)-H(4)···O(1) = 2.114(18) Å, N(4)···O(1) = 2.945(2) Å, ∠N(4)-H(4)···O(1) = 160(2)°). The dimeric association is supported by inter-pair π-π interactions brought on by intermolecular anti-parallel stacking involving Hdpa ligands. The π-π stacking between C(20) of py and C(21) of py (C(20)···C(21) = 3.281(4) Å) rings of neighboring coordinated Hdpa ligand ($C_g(p)\cdots C_g(p)$ (3.502(4) Å) is expected to stabilize the complex in the solid state. At a centroid contact of 3.502(4) Å and angle of 21.99(4)° between the ring normal and the centroid vector corresponds to horizontal displacement of 1.383(4) Å reveals the shift of almost one C-C bond length face-to-face alignment ($C_g(p)$). Therefore, the stacked Hdpa ligands show the Cu···Cu separation as 6.551(3) Å.

3.3. Electronic spectra

The electronic spectra of **1** in MeOH and MeOH:H_2O (4:1 v/v) are very similar and display a broad ligand-field band (λ_{max}, 651 nm) with a weak low-energy shoulder (λ_{max}, 897

nm) in the visible region and the intensity of higher energy band (ε_{max}, 202 $M^{-1}cm^{-1}$) is significantly higher than the intensity of lower energy shoulder (ε_{max}, 70 $M^{-1}cm^{-1}$), which is characteristic for distorted square pyramidal copper(II) complexes [28,29]. The diffuse reflectance spectrum of **1** exhibits the broad ligand-field band (λ_{max}, 653 nm) suggesting the possibility of an oxygen atom coordinated to copper(II). The position of the band remains almost unchanged in the solid-state when compared with the solution spectrum indicating that the complex retains in solutions its solid-state coordination geometry [30] determined by X-ray crystallography (distorted square pyramidal). The intense absorption band observed in the UV region (λ_{max}, 249-310 nm) is attributed to the intraligand π-π^* transition in the coordinated diimines. The low-intensity band (λ_{max}, 393 nm) is assigned to naphtholate anion to copper(II) ligand-to-metal charge-transfer (LMCT) transition, revealing the involvement of the naphtholate oxygen atom in coordination even in solution.

3.4. EPR spectra

The EPR spectrum of **1** exhibit one broad singlet (g_{iso} = 2.078) in the polycrystalline state at 298 K arising from dipolar broadening and enhanced spin-lattice relaxation. In frozen solutions of **1**, three of the four parallel hyperfine features were well separated while the fourth one overlapped with the perpendicular features in DMF whereas the parallel feature was very weakly resolved and the perpendicular feature was moderately broader in MeOH (g_{iso}, 2.128) and in MeCN (g_{iso}, 2.083), the signals were significantly broader (Fig. 2). This suggests that the dimeric intermolecular association is retained in weak coordinating solvents like MeCN and MeOH [31] while strong coordinating solvent like DMF, the association is disturbed due to solvolysis.

The frozen DMF solution EPR spectrum of **1** shows axial spectral features typical of mononuclear Cu(II) species ($g_{\|}>g_{\perp}>2.0$; $G = (g_{\|}-2) / (g_{\perp}-2) = 5.2$) suggesting the presence of $d_{x^2-y^2}$ ground state in copper(II) located in square-based geometries [18]. Further, a square-based CuN_4 chromophore is expected [32,33] to show $g_{\|}$ (2.200) and $A_{\|}$ (180-200 × 10^{-4} cm^{-1}) values and the replacement of a nitrogen atom in this chromophore by an oxygen atom and incorporation of strong axial interaction has been found to increase the $g_{\|}$ and decrease the $A_{\|}$ values [34]. Therefore, the observed $g_{\|}$ (2.227) and $A_{\|}$ (188 × 10^{-4} cm^{-1}) values are consistent with the presence of a square-based CuN_3O chromophore with strong axial interaction (cf. above). The value of $g_{\|}/A_{\|}$ (118 cm) quotient indicates appreciable distortion of the structure, which is borne out by the value of the trigonality index, τ. Molecular orbital coefficients [35], α^2 (a measure of the covalency of the in-plane σ-bonding between 3d orbital and the ligand orbitals)

and β^2 (covalent in-plane π-bonding) were estimated and the α^2 (0.80) and β^2 (0.65) values indicate that there is a substantial interaction in the in-plane σ-bonding whereas the in-plane π-bonding is almost covalent. For complex **1**, it is observed that $K_{\|} > K_{\perp}$ [36] ($K_{\|}$ (0.72) and $K_{\perp}$ (0.63) are orbital reduction factors), showing the significant out-of-plane π-bonding.

3.5. Redox properties

Cyclic (CV) and differential pulse voltammetric (DPV) responses of **1** obtained from MeOH reveal the electrochemically and chemically reversible Cu^{II}/Cu^{I} redox behavior, as apparent from the linear plot of i_{pc} versus $\nu^{1/2}$ (D, 5.2×10^{-6} cm^2 s^{-1}) and the values acquired for peak current ratio (i_{pa}/i_{pc}, 2.4; reaches unity by increasing the scan rate) respectively. However, the value of the limiting peak-to-peak separation (ΔE_p, 67 mV), which is smaller than that for the Fc/Fc^+ couple (ΔE_p, 86 mV; $E_{1/2}$, 0.406 V vs SCE) under identical conditions. Interestingly, it exhibits low ΔE_p (67 mV) and positive Cu(II)/Cu(I) redox potential ($E_{1/2}$, 0.159 V vs SCE), which signifies that the structural reorganization between their copper(II) and copper(I) species is minimal leading to a facile heterogeneous electron transfer [37] possibly due to the formation of boat conformation in six-membered chelate ring (Cu-O-C-C-C-N) induced by the steric clash between -NMe_2 group in H(L) and non-planar Hdpa ligand (cf. τ values, 0.12).

3.6. Ascorbic acid oxidation

Interestingly, the addition of ascorbic acid (H_2A) to the green solution of catalyst **1** (3×10^{-3} M) did not change to the brown solution and no new CT band is observed (Fig. 3). Instead, the d-d band undergoes blue shift (λ_{max}: 649 to 634 nm), indicating the coordination of one of the oxygen donors (H_2A) with a square pyramidal complex **1** (ESI-MS positive (Fig. S6): m/z, 673.35 confirms the formation of an adduct, $\{Na\text{-}[Cu^{II}(L)(Hdpa)(ascorbate\ ion)]\}^+$ and the peaks are found at m/z, 474.50 and 950.85 corresponds to monomeric unit, $[Cu^{II}(L)(Hdpa)]^+$, and dimeric aggregate, $2[Cu^{II}(L)(Hdpa)]^+$, of the complex respectively), which is consistent with octahedral geometry. This is possible because of the centrosymmetric dimer consists of two stable six-membered chelate rings (Cu(1)N(3)C(20)N(4)C(21)N(5)) in the anti-parallel slip orientation due to the rapid flapping of the py rings of Hdpa in the opposite direction. This could destroy the steric match between H_2A and catalyst (**1**) in order to prevent the oxidation of ascorbic acid to dehydroascorbic acid.

3.7. Benzylamine oxidation

The catalytic reaction of benzylamine (100×10^{-3} M) using complex **1** (1×10^{-3} M) as a catalyst in the presence of H_2O_2 (1 ml of 30% w/v) in 10 ml of MeOH:H_2O (4:1 v/v) causes the complete oxidation of benzylamine to benzaldehyde ($PhCH_2NH_2 \rightarrow PhCHO + NH_3$). The

formation of the reaction products is evidenced by the ^{1}H NMR (Fig. S7: benzylamine, -CH_2-, δ 3.872 ppm; benzaldehyde, -CHO, δ 10.032 ppm) and mass (Fig. S8: shows two peaks at m/z, 105.9 and 107.0 assignable to [$PhCO^+$+H] and [PhCHO+H] respectively) spectral studies. The proposed catalytic cycle reveals that the initial step of the catalytic reaction is the formation of an adduct showing a significant shift of the visible band (λ_{max}: 643 to 595 nm) to higher energy (Fig. 4) by the addition of benzylamine to the solution of **1**. This adducts species react with H_2O_2 to form an initial brown color solution that does not show any d-d band. It indicates the one-electron reduction of copper along with the concomitant protonation of the L ligand by benzylamine adduct with copper. Thus, the copper(I) species is reactive towards benzylamine which undergoes oxidation to benzylimine and the presence of water hydrolyzes benzylimine to benzaldehyde.

3.8. Catechol oxidation

The reactivity of copper(II) complex, **1** (2.9×10^{-5} M) in methanol towards the aerobic oxidation of 3,5-di-*tert*-butylcatechol (3,5-$DTBCH_2$; 50 equivalent) was repeatedly monitored by the improvement of the strong band at 393 nm for every 30 min time interval during the course of a reaction (Fig. 5). It reveals the development of a strong absorption band at 393 nm characteristic of quinone chromophore (3,5-di-*tert*-butyl-*o*-quinone; 3,5-DTBQ), which prompt us to conclude that **1** is reactive towards catecholase activity. The same reaction was done by scaling up the reactants and the desired 3,5-DTBQ was isolated column chromatographically using 10% mixture of ethyl acetate and hexane as eluent. The isolated *o*-quinone was identified by ^{1}H NMR spectra in $CDCl_3$ (Fig. S9: -CH_3 (C), s, δ 1.229 ppm, 9H; -CH_3 (D), s, δ 1.272 ppm, 9H; H (B), s, δ 6.220 ppm, 1H; H (A), s, δ 6.936 ppm, 1H). The kinetic data were determined by the method of initial rates by monitoring the growth of the 393 nm band of the product 3,5-DTBQ for the first 3 h, formed due to the oxidation of 3,5-$DTBCH_2$ (5-45 equivalents) in the presence of **1** (2.9×10^{-5} M). A treatment on the basis of the Michaelis-Menten model is appropriate and Lineweaver-Burk plot for **1** gave straight line (Fig. 6), from which the kinetic parameters such as maximum velocity (V_{max}, 6.9×10^{-4} M min^{-1}), Michaelis binding constant (K_M, 12.2×10^{-5} M) and the turnover number (k_{cat}, 1424 h^{-1}) were evaluated. Interestingly, the k_{cat} is superior to the other mono and binuclear complexes (k_{cat}, 33-925 h^{-1}) [38]. Also, we found the band at 353 nm which is due to the existence of I_3^- [39], provides evidence for the formation of H_2O_2 from the reaction mixture. In order to understand the catalytic oxidation of 3,5-$DTBCH_2$ to 3,5-DTBQ, the electrospray ionization mass spectrum (ESI-MS positive) of a mixture of **1** and 3,5-$DTBCH_2$ (molar ratio, 1:10) was recorded after 30 min in methanol solution (Fig. 7). The

most abundant species found at m/z = 476.75 arises from a monomeric unit of the complex and are assigned to $[Cu^{II}(L)(Hdpa)]^+$. The low intense peak at m/z = 952.45 appears due to the dimeric aggregate of the complex, which can be assigned to $2[Cu^{II}(L)(Hdpa)]^+$ indicating the existence of the self-assembled molecular association of **1** in solution and substantiating the results from the frozen solution EPR spectra in MeOH and MeCN (cf. above). The peak at 243.30 is well assignable to the $[3,5\text{-DTBQ-Na}]^+$. The remaining peak at m/z = 721.80 including two additional peaks at m/z = 753.35 and 1197.30 are observed, which clearly indicate that these peaks arise from complex-substrate aggregates and can be assigned to $\{Na\text{-}[Cu^{I}(HL)(Hdpa)(3,5\text{-DTBCH})]\}^+$, $\{Na\text{-}[Cu^{II}(HL)(Hdpa)(O_2)(3,5\text{-DTBCH})]\}^+$ and $\{Na\text{-}[Cu^{II}(HL)(Hdpa)]\text{-}(3,5\text{-DTBC})\text{-}[Cu^{II}(HL)(Hdpa)]\}^{3+}$ respectively.

4. Conclusion

Most noteworthy about the catalytic results is the fact that the efficient catalysis is influenced by square pyramidal (4+1) coordination geometry with the labile binding site of the complex. It is also assumed that a close steric match between the substrate and the copper ion is of crucial importance for efficient catalysis to occur [40]. It has been shown that electron transfer from substrate to copper(II) can begin only after the substrate and copper(II) species form copper(II)-substrate intermediate like 'enzyme-substrate' complex [41]. The copper(II) complex (**1**) possesses square pyramidal (4+1) coordination geometry and its crystal packing reveals the formation of the centrosymmetric dimer held together by self-assembled molecular association (N-H···O and inter-pair π-π). Interestingly, the existence of the dimeric intermolecular association in solution is evidenced by the frozen EPR and ESI-MS solution studies. The dimeric aggregate of the complex does not have the steric match between the bulky ascorbic acid and copper(II) ion, which prevents the formation of copper(II)-ascorbate intermediate. However, the enhanced catalytic activity takes place in the case of compact benzylamine or catechol with **1** due to the easy formation of copper(II)-substrate intermediate, indicating the close steric match between the substrate and the catalyst. Thus, the self-assembled molecular association determines that **1** behaves as a functional model for amine and catechol oxidases but not for ascorbate oxidase.

Acknowledgments

We thank the Science and Engineering Research Board, New Delhi (Grant No. EMR/2016/007756) for financial support. Thanks are due to STIC, Cochin University of Science

and Technology for X-ray crystal structure data. We thank SAIF, Indian Institute of Technology Madras for structure solution and refinement (Dr. P. K. Sudhadevi) and for recording EPR spectra. This paper is dedicated to Dr. R. Brakaspathy, (Former Secretary, SERB, New Delhi, India) Research and Development Advisor, Indian Institute of Technology Madras, Chennai, India on the occasion of his 62nd birthday.

Appendix A. Supplementary data

Crystallographic data for the structural analysis of [Cu(L)(Hdpa)](ClO_4) (**1**) have been deposited with Cambridge Crystallographic Data Center, CCDC No. 1861819. Copies of this information may be obtained free of charge from http://www.ccdc.ac.uk/const/retrieving.html or from the CCDC, 12 Union Road, Cambridge, CB2 1EZ, UK (email: deposit@ccdc.cam.ac.uk). Supplementary data associated with this article can be found, in the online version, at …….

References

[1] M. Rolff, J. Schottenheim, H. Decker, F. Tuczek, Chem. Soc. Rev. 40 (2011) 4077-4098.
[2] S. Friedle, E. Reisner, S.J. Lippard, Chem. Soc. Rev. 39 (2010) 2768-2779.
[3] L. Que Jr., W.B. Tolman, Nature 455 (2008) 333-340.
[4] A. Messerschmidt, A. Rossi, R. Ladenstein, R. Huber, M. Bolognesi, G. Gatti, A. Machesini, R. Petruzzelli, A. Finazzi-Agró, J. Mol. Biol. 206 (1989) 513-529.
[5] A. Messerschmidt, R. Ladenstein, R. Huber, J. Mol. Biol. 230 (1993) 997-1014.
[6] C.M. Chang, V.J. Klema, B.J. Johnson, M. Mure, J.P. Klinman, C.M. Wilmot, Biochemistry 49 (2010) 2540-2550.
[7] M.R. Parsons, M.A. Convery, C.M. Wilmot, K.D.S. Yadav, V. Blakeley, A.S. Corner, S.E.V. Phillips, M.J. McPherson, P.F. Knowles, Structure 3 (1995) 1171-1184.
[8] I.A. Koval, P. Gamez, C. Belle, K. Selmeczi, J. Reedijk, Chem. Soc. Rev. 35 (2006) 814-840.
[9] A.L. Hughes, Immunogenetics 49 (1999) 106-114.
[10] C. Gerdemann, C. Eicken, B. Krebs, Acc. Chem. Res. 35 (2002) 183-191.
[11] M. Guell, P.E.M. Siegbahn, J. Biol. Inorg. Chem. 12 (2007) 1251-1264.
[12] B.T.O. Holt, M.A. Vance, L.M. Mirica, D.E. Heppner, T.D.P. Stack, E.I. Solomon, J. Am. Chem. Soc. 131 (2009) 6421-6438.
[13] S. Kr Dey, A. Mukherjee, Coord. Chem. Rev. 310 (2016) 80-115.
[14] A. Biswas, L.K. Das, M.G.B. Drew, C. Diaz, A. Ghosh, Inorg. Chem. 51 (2012) 10111-10121.
[15] G. Grigoropoulou, K.C. Christoforidis, M. Louloudi, Y. Deligiannakis, Langmuir 23 (2007) 10407-10418.
[16] Á. Kupán, J. Kaizer, G. Speier, M. Giorgi, M. Réglier, F. Pollreisz, J. Inorg. Biochem. 103 (2009) 389-395.
[17] D. Jiang, X. Li, L. Liu, G.B. Yagnik, F. Zhou, J. Phys. Chem. B 114 (2010) 4896-4903.
[18] Z. Moradi-Shoeili, Z. Amini, D.M. Boghaei, B. Notash, Polyhedron 53 (2013) 76-82.
[19] S. Sarkar, A. Sim, S. Kim, H. Lee, J. Mol. Cat. A-Chem. 410 (2015) 149-159.
[20] V. Sathya, M. Murali, Inorg. Chem. Commun. 92 (2018) 55-59.
[21] B.K. Santra, P.A.N. Reddy, M. Nethaji, A.R. Chakravarty, Inorg. Chem. 41 (2002) 1328-

1332.
[22] P. Jaividhya, R. Dhivya, M.N. Akbarsha, M. Palaniandavar, J. Inorg. Biochem. 114 (2012) 94-105.
[23] B.-T. Ko, C.-C. Chang, S.-L. Lai, F.-J. Lai, C.-C. Lin, Polyhedron 45 (2012) 49-54.
[24] Bruker, APEX2, SAINT and SADABS, AXS Inc., Madison, Wisconsin, USA, 2004.
[25] G.M. Sheldrick, Acta Cryst. Sect. A 64 (2008) 112-122.
[26] G.M. Sheldrick, Acta Cryst. Sect. C 71 (2015) 3-8.
[27] A.W. Addison, T.N. Rao, J. Reedijk, J. Van Rijn, G.C. Verschoor, J. Chem. Soc., Dalton Trans. (1984) 1349-1356.
[28] B.J. Hathaway, D.E. Billing, Coord. Chem. Rev. 5 (1970) 143-207.
[29] R. Marion, N.M. Saleh, N.L. Poul, D. Floner, O. Lavastre, F. Geneste, New. J. Chem. 36 (2012) 1828-1835.
[30] E.V. Rybak-Akimova, A. Y. Nazarenko, L. Chen, P. W. Krieger, A. H. Herrera, V.V. Tarasov, P.D. Robinson, Inorg. Chim. Acta 324 (2001) 1-15.
[31] P.S. Subramanian, E. Suresh, P. Dastidar, S. Waghmode, D. Srinivas, Inorg. Chem. 40 (2001) 4291-4301.
[32] P. Tamil Selvi, M. Murali, M. Palaniandavar, M. Kockerling, G. Henkel, Inorg. Chim. Acta 340 (2002) 139-146.
[33] C. Rajarajeswari, R. Loganathan, M. Palaniandavar, E. Suresh, A. Riyasdeen, M.A. Akbarsha, Dalton Trans. 42 (2013) 8347–8363.
[34] R. Loganathan, S. Ramakrishnan, E. Suresh, A. Riyasdeen, M.A. Akbarsha, M. Palaniandavar, Inorg. Chem. 51 (2012) 5512-5532.
[35] E. Turkkan, U. Sayin, N. Erbilen, S. Pehlivanoglu, G. Erdogan, H.U. Tasdemir, A.O. Saf, L. Guler, E.G. Akgemci, J. Organomet. Chem. 831 (2017) 23-25.
[36] A.S. El-Tabl, M. Abd-Elwahed, M.H. Mohammed, Chem. Spec. Bioavailab. 25 (2013) 133-146.
[37] R. Balamurugan, M. Palaniandavar, H. Stoeckli-Evans, M. Neuburger, Inorg. Chim. Acta 359 (2006) 1103-1113.
[38] E.C.M.O. Wenker, M.A. Siegler, M. Lutz, E. Bouwman, Dalton Trans. 44 (2015) 12196-12209.
[39] P. Adak, B. Ghosh, A. Bauzá, A. Frontera, A.J. Blake, M. Corbella, C.D. Mulhopadhyay, S.K. Chattopadhyay, RSC Adv. 6 (2016) 86851-86861.
[40] P.S. Subramanian, E.suresh, P. Dastidar, Polyhedron 23 (2004) 2515-2522.
[41] S. Mondal, M. Chakraborty, A. Mondal, B. Pakhira, A.J. Blake, E. Sinn, S.K. Chattopadhyay, New J. Chem. 42 (2018) 9588-9597.

HIGHLIGHTS

- Possess square pyramidal (4+1) coordination geometry
- Display two types of self-assembled intermolecular associations
- No catalytic activity towards the oxidation of ascorbic acid
- Effective catalyst towards the oxidation of benzylamine and 3,5-di-*tert*-butylcatechol
- Functional Model for Cu(II) sites in type-2 and type-3 copper oxidases

Graphical Abstract

Mononuclear copper(II) complex [Cu(L)(Hdpa)](ClO_4) possesses CuN_4O chromophore. It shows good catalytic activity towards the oxidation of benzylamine and 3,5-di-*tert*-butylcatechol due to the existence of self-assembled molecular association, in turn, favors steric match between catalyst and substrate.

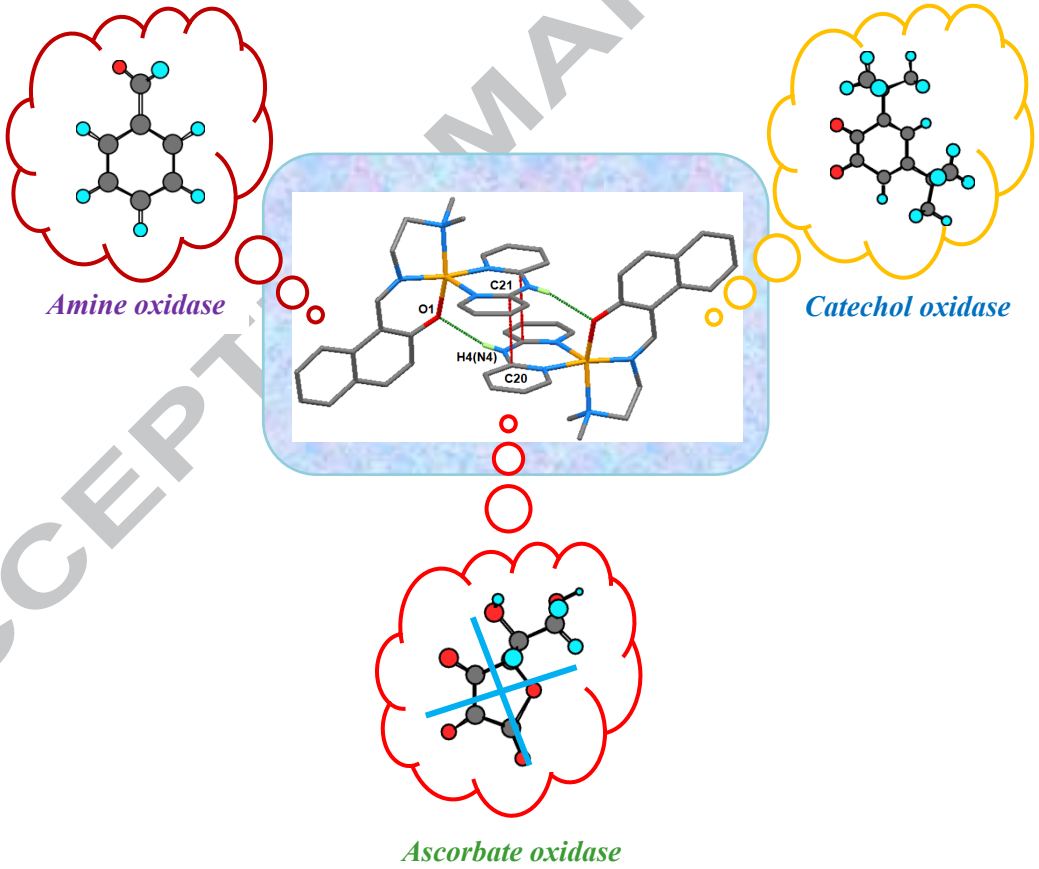

Legends for figures

Scheme 1 Structure of ligands (H(L) obtained from the condensation of 2-hydroxy-1-naphthaldehyde and N,N-dimethylethylenediamine and Hdpa is 2,2'-dipyridylamine)

Fig. 1 (a) ORTEP diagram of $[Cu(L)(Hdpa)]^+$ (**1**) showing 40% probability thermal ellipsoids with the atom labeling scheme for the metal, heteroatoms and disorded C(1), C(1)', C(2), C(2)', C(3), C(3)', C(4), C(4)' atoms in *N*,*N*-dimethylethylenediamine moiety and (b) Packing diagram viewed down the *a*-axis showing intermolecular interactions (Symmetry code: -x+1, -y, -z+2) of $[Cu(L)(Hdpa)]^+$ (**Green**, N-H···O bonding; **Red**, π-π stacking). The disordered perchlorate anion is omitted for clarity.

Fig. 2 EPR spectra for frozen solutions of $[Cu(L)(Hdpa)](ClO_4)$ (**1**) at 77K: (a) DMF, (b) MeOH and (c) MeCN.

Fig. 3 Visible spectral traces showing the conversion of $[Cu(L)(Hdpa)](ClO_4)$ (**1**) (3×10^{-3} M) (a) to (b) on coordination with ascorbic acid (3×10^{-3} M) in MeOH:H_2O (4:1 v/v). Inset: No conversion of the copper(I) species.

Fig. 4 Visible spectra of $[Cu(L)(Hdpa)](ClO_4)$ (**1**) in MeOH:H_2O (4:1 v/v) (a), in presence of benzylamine (b) and after treatment with benzylamine and H_2O_2 (c).

Fig. 5 Oxidation of 3,5-$DTBCH_2$ by $[Cu(L)(Hdpa)](ClO_4)$ (**1**) in MeOH monitored by UV-Vis spectroscopy.

Fig. 6 Dependence of reaction rates on the 3,5-$DTBCH_2$ concentration for the oxidation reaction catalyzed by $[Cu(L)(Hdpa)](ClO_4)$ (**1**). Inset: Lineweaver-Burk plot.

Fig. 7 ESI-Mass spectrum recorded for the reaction between 3,5-$DTBCH_2$ and **1**, after 30 minutes.

Scheme 1

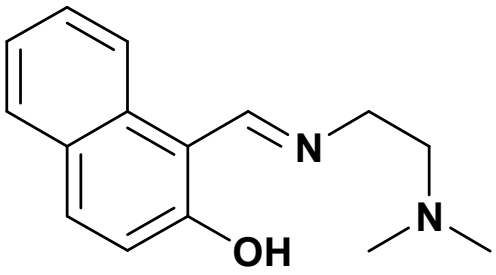

H(L)

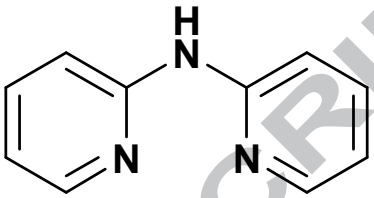

Hdpa

Fig. 1

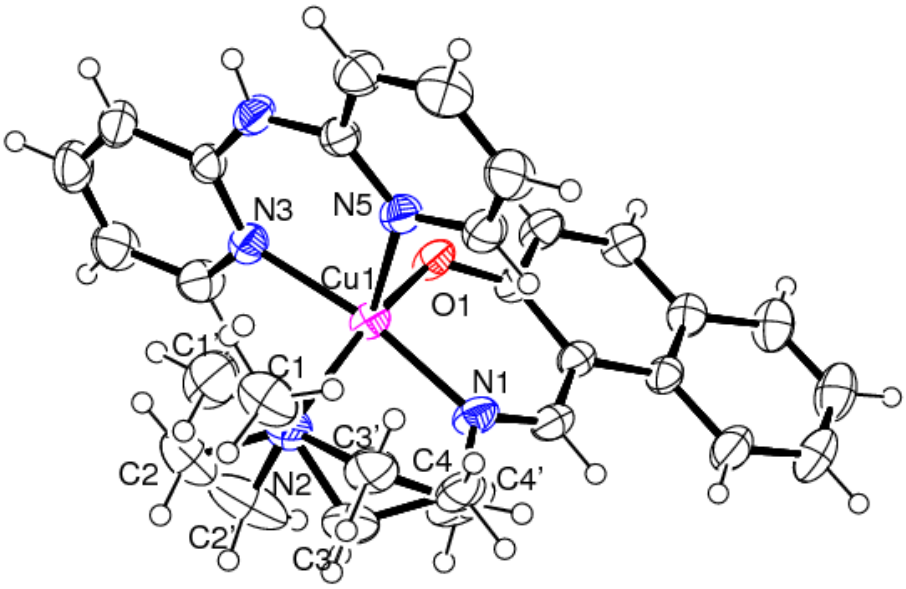

(a)

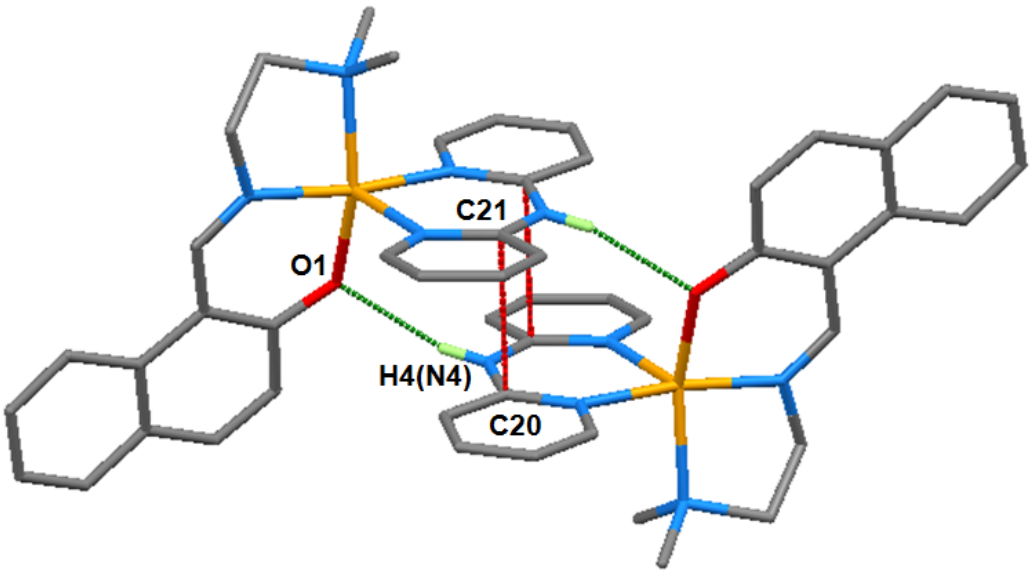

(b)

Fig. 2

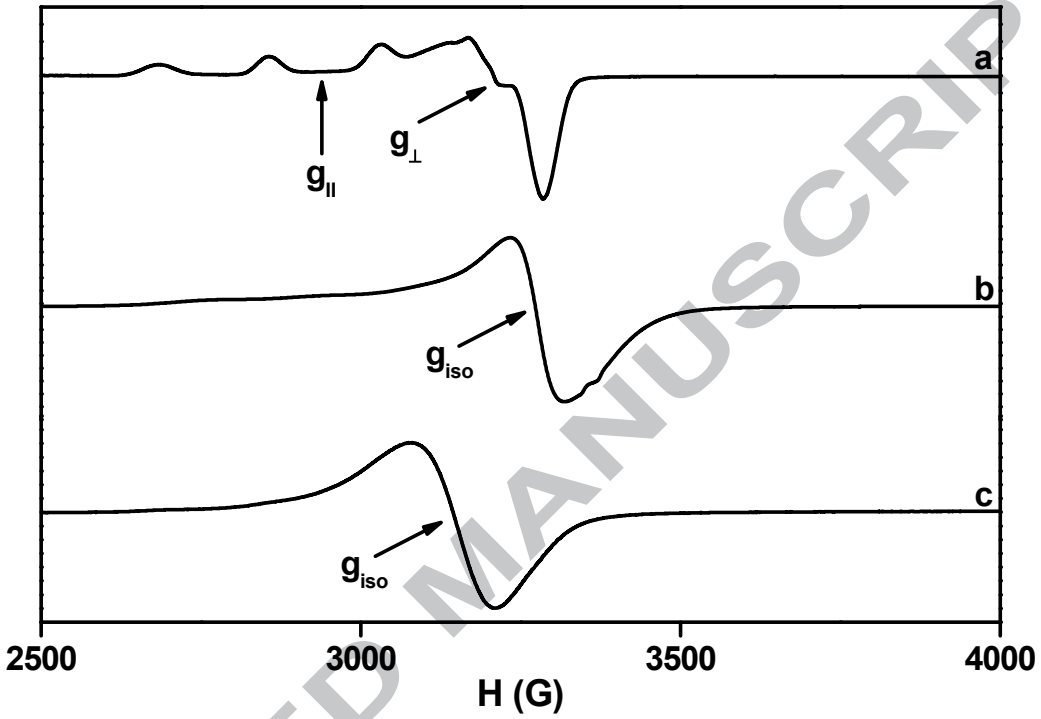

Fig. 3

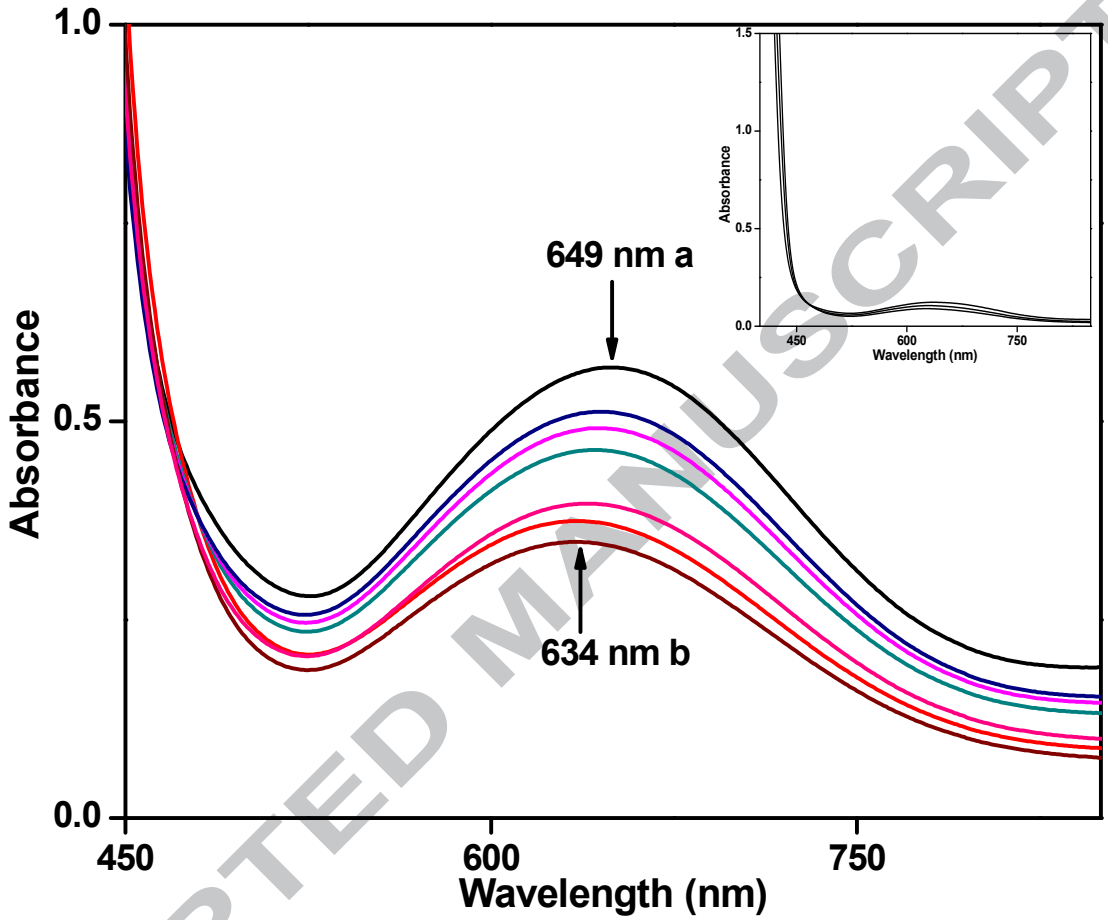

Fig. 4

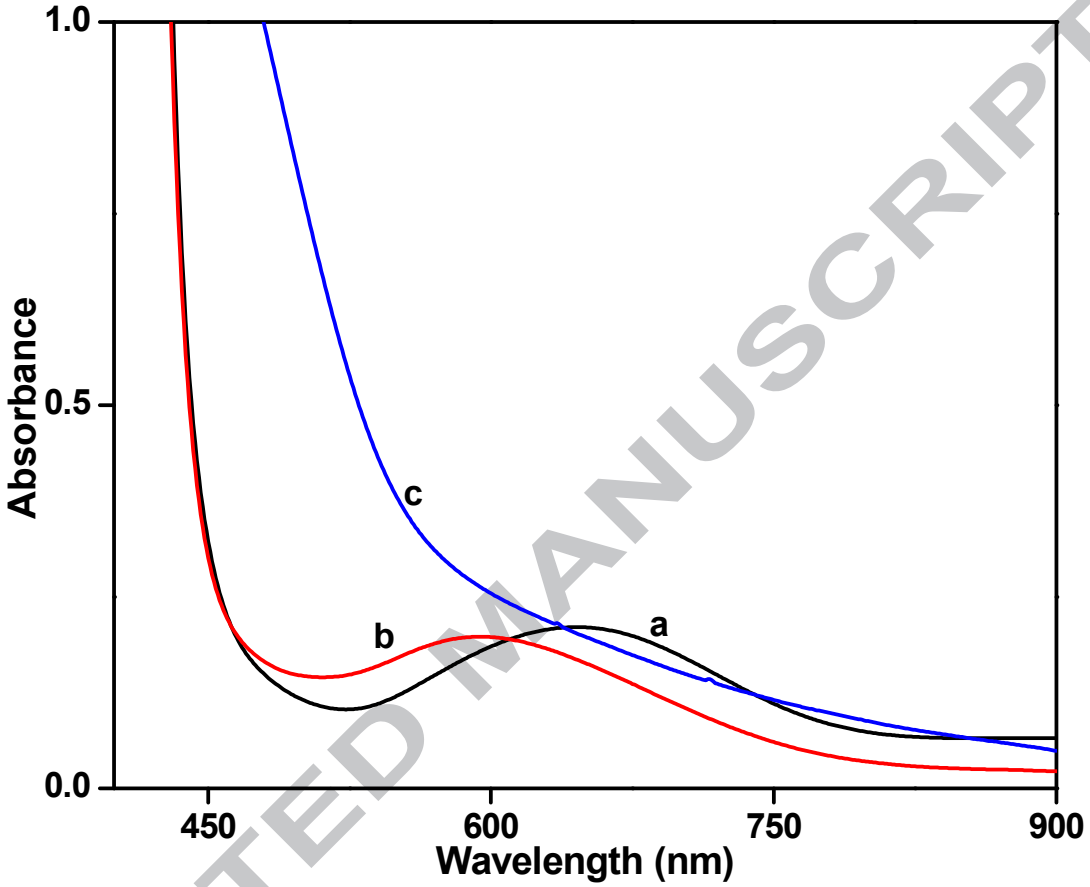

Fig. 5

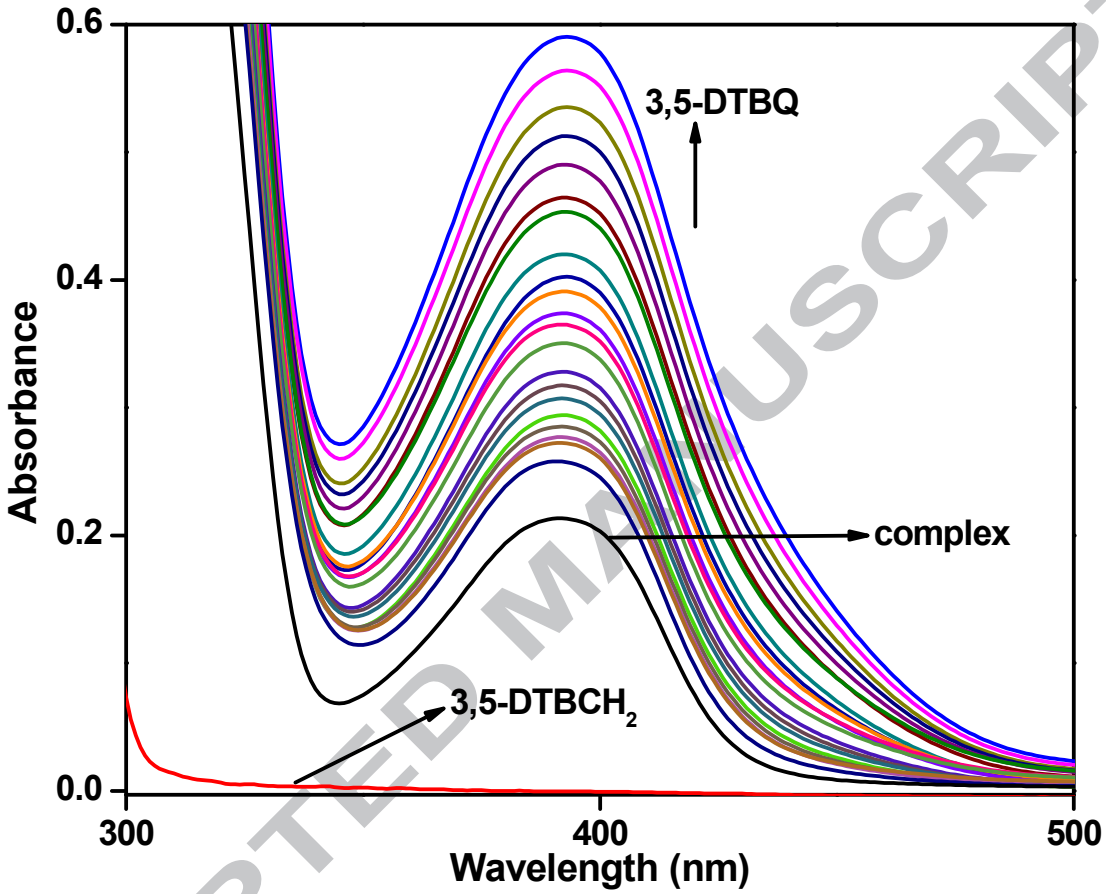

Fig. 6

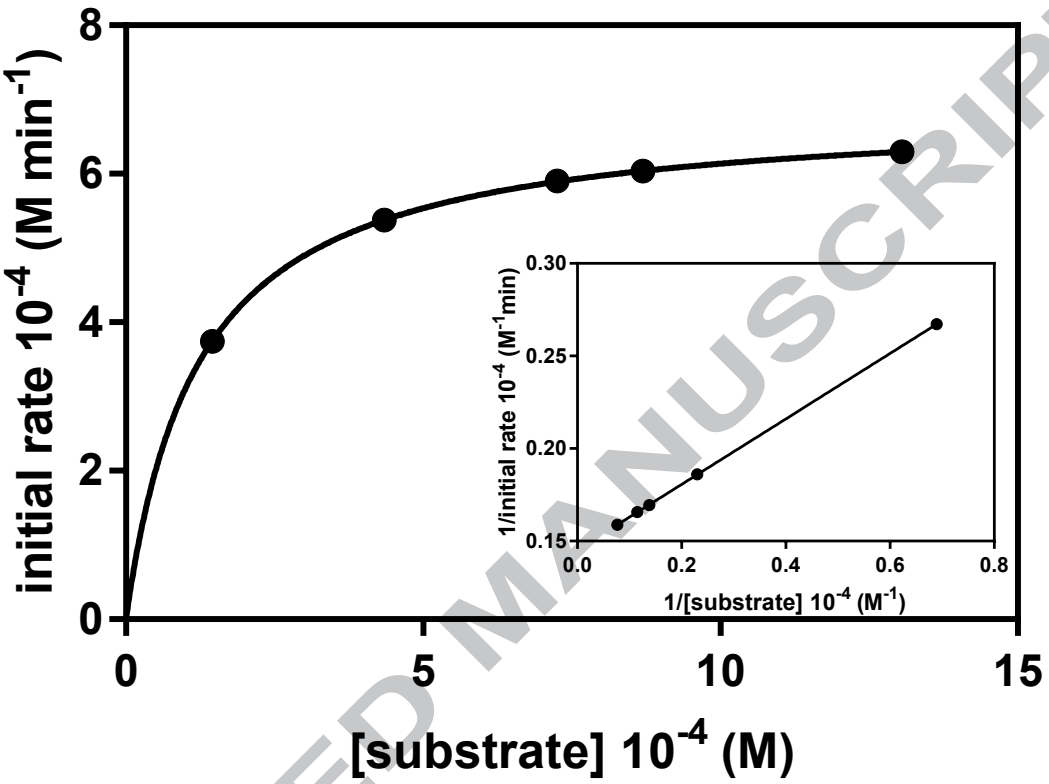

Fig. 7

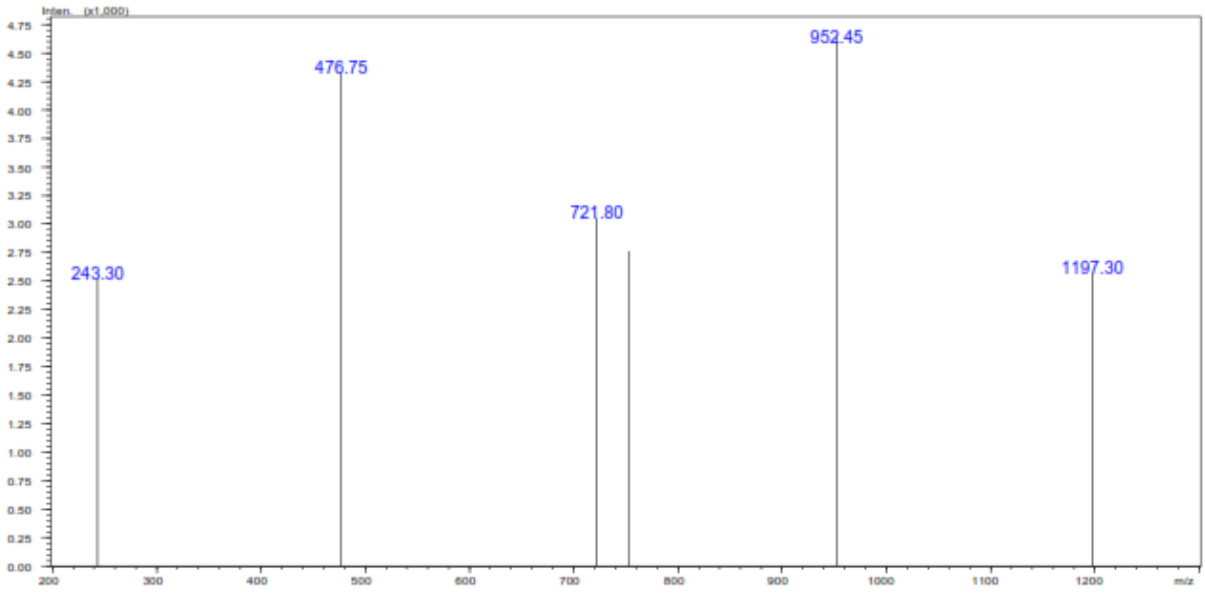

Table 1
Selected crystal data and structure refinement parameters for [Cu(L)(Hdpa)](ClO_4) (**1**)

Formula	$C_{25}H_{26}ClCuN_5O_5$
Formula weight	575.50
Temperature (K)	296(2)
Wavelength (Å)	0.71073
Crystal system	Monoclinic
Space group	$P2_1/c$
a (Å)	9.0434 (2)
b (Å)	17.7067 (5)
c (Å)	15.8463 (4)
α (°)	90
β (°)	100.2410 (10)
γ (°)	90
V (Å)^3, Z	2497.02 (11), 4
D_{calc} (g cm^{-3})	1.531
μ (mm^{-1})	1.029
F(000)	1188
Crystal size (mm)	0.30 × 0.25 × 0.20
θ (°)	2.56-28.17
Index ranges	-11≤h≤9, -23≤k≤23, -20≤l≤20
Reflections collected	28648
Independent reflections	6049
Reflections observed [I > 2σ(I)]	4513
R_{int}	0.0324
GOOF	1.015
R_1 [I > 2σ(I)]	0.0359
wR_2 [I > 2σ(I)]	0.0951
R_1/wR_2 all data	0.0564/0.1070

Table 2
Selected bond lengths (Å) and bond angles (°) for [Cu(L)(Hdpa)](ClO_4) (**1**)

Cu(1)-N(1)	1.9230(18)	Cu(1)-N(2)	2.1338(19)
Cu(1)-N(3)	1.9979(18)	Cu(1)-N(5)	2.1805(18)
Cu(1)-O(1)	1.9567(15)		
O(1)-Cu(1)-N(1)	91.04(7)	O(1)-Cu(1)-N(2)	160.32(7)
O(1)-Cu(1)-N(3)	88.54(7)	O(1)-Cu(1)-N(5)	103.05(7)

N(1)-Cu(1)-N(2)	83.38(8)	N(1)-Cu(1)-N(3)	167.40(8)
N(1)-Cu(1)-N(5)	103.26(7)	N(2)-Cu(1)-N(3)	92.85(7)
N(2)-Cu(1)-N(5)	96.60(7)	N(3)-Cu(1)-N(5)	89.09(7)